Methods for Assessing Changes in the fMRI Visual Field Map after Surgery

Raymond G. Hoffmann[1], Mary Jo Macjewskii[1,2], Paul Savarapian[3], Edgar A. DeYoe[1], Daniel Rowe[1]
Medical College of Wisconsin[1], Marquette University[2], Northwestern College (Iowa)[3]
hoffmann@mcw.edu

Abstract

The visual field map is produced by mapping the active voxels of the visual cortex to a circular region corresponding to the points of the circular image. Activation of the voxels is determined by matching the fMRI time series to a time series based on a complex visual stimulus consisting of rotating wedges and rings expanding from the center to the boundary of the disk.

Each scan (pre-surgical, post-surgical) produces a different set of points due to due to noise in the fMRI response to the visual target, hemodynamic variability and variability in the position of the head between scans and . A spatial-temporal non-homogeneous Poisson process is used to model the density of the active voxels. The differential density of the voxels reflects the differences in density of the optical sensors in the retina from the center to the periphery. Two types of changes may occur post-surgery: (1) thinning of the response or (2) actual "holes" in the visual response.

Using data obtained from healthy patients, surgery was simulated with full scans as well as known masks (18o to 90o wedges) as well as randomly thinned areas (180o and 360o), we examined the sensitivity and specificity of different spatial methods for identifying pre-post surgical changes: (1) nearest neighbor, (2) emptiness measures, (3) spatial intensity measures and (4) goodness of fit to an empirical model

Keywords: point process, spatial statistics, fMRI

1. The Visual Field Map Generates a Point Process

The visual field diagram is formed by an **inverse mapping** of areas of the visual cortex to the retinotopic area stimulated by an array of visual targets. The visual targets are a series of concentric circles that illuminated in sequence. The corresponding blood flow in the visual cortex is imaged by BOLD fMRI. The Bold fMRI signal is correlated with the stimulus. In particular the time delay in the fMRI signal is used to identify which of the concentric circles is being illuminated as is shown in Figure 1. Each color represents a region of the visual cortex (Figure 2) that corresponds to a region of the retina activated by the visual target. Blue is the area of the visual cortex that corresponds to the innermost circle.
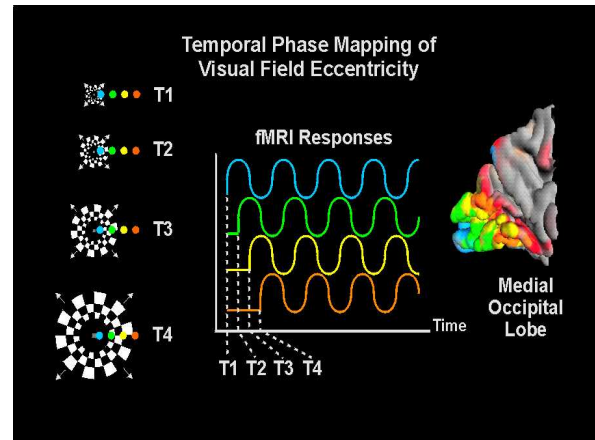
Figure 1. Presentation of the targets over time leads to a mapping of the visual cortex.
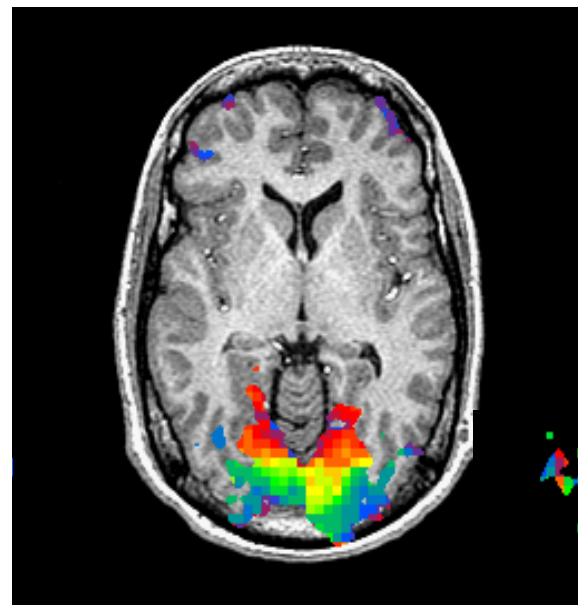
Figure 2. Functional Activation showing visual field eccentricity (distance from center of gaze) represented by different colors calculated from the delay of the fMRI signal.

The target also rotates as in Figure 3. The combination of the rotational segment and the concentric circle gives a location in the visual field for each of the voxels in the visual cortex. Figures 1 through 3 are from DeYoe, 1996 and DeYoe, 1997.

1.1 Secondary Subhead Flush Left in Title Case in 10-Point Bold Type
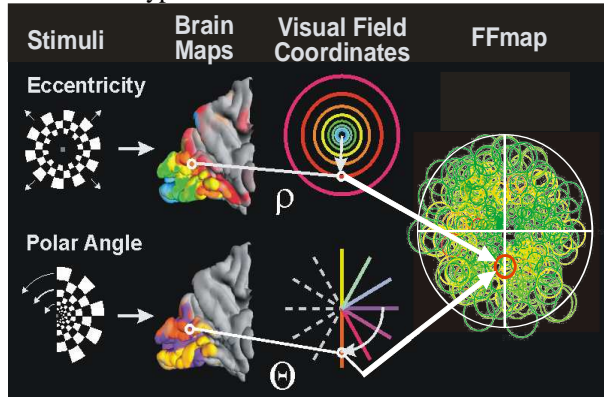
Figure 3. Location of the points in the visual fields. A point is present only if the correlation between the fMRI BOLD signal and the pattern is above a threshold that is kept constant for all scans in a study.

Patients with epilepsy that cannot be controlled by medication, will have surgery to control the condition. Since the regions that are resected in surgery lie near to the regions of the brain that affect the visual subsystem, an important problem is the determination of what portion of the visual field was affected by the surgery.

2. Simulated Effects of Surgery

In order to quantitate this process, a statistical model for changes in the visual field is necessary. In order to test this model, simulated changes in the visual field were constructed by masking part of the visual stimulus.

To "simulate" the effect of surgery, 0, 18, 27, 36, 45 and 90 degree wedges were used to mask part of the visual field when the data was collected from a subject. Figure 4 shows the different sizes of the masks and the corresponding effects on the points in the visual field. Figure 4 is from Maciejewski, 2005.

The retina of the eye has a greater sensitivity in its center area corresponding to a greater density of rods and cones. This is reflected in the greater density of activated points in the center of the visual field maps(Figure 5).
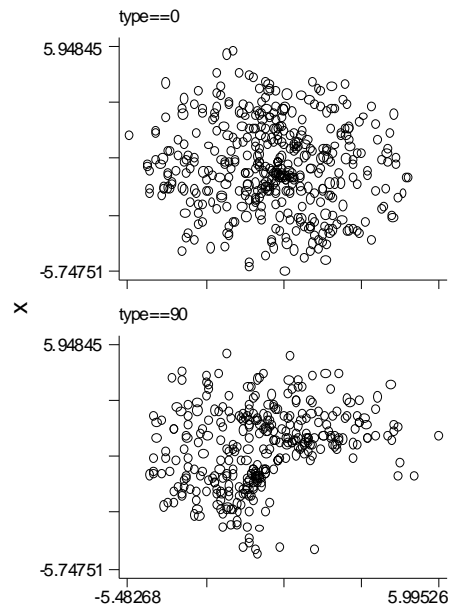
Figure 5. Points in the full (top) and 90° mask (bottom). Note that each scan is a separate realizations of a stochastic process.

Because of the winner take all algorithm that generates the FF map and noise inherent in fMRI scanning, the resulting map has random points in the area masked by

Full stimulus	90 degree mask	45 degree mask	36 degree mask	27 degree mask	18 degree mask

the wedge. Each scan produces a similar, but random, set of points.

Since potential damage to the visual field in clinical subjects could be global rather than local, we also used random thinning applied to all the points of the 0 degree wedge to simulate global damage. The random thinning was applied to the entire visual field with a 0.50 and a 0.75 proportion of all the points kept. In addition, a 50% thinning of the left half of the visual field was also used.

Figure 5 shows the effect of a 90 degree mask on the points of the visual field map for a single subject. Figure 6 shows the effect of randomly thinning the points by 50%.
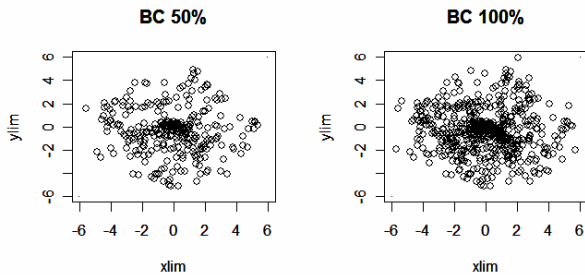
Figure 8. Simulated effect of a 50% thinning of all the points in the visual field.

2.1 The Statistical Model

The underlying statistical model is a non-homogeneous Poisson process. While the general model is similar for each subject; namely, a higher spatial intensity in the center of the visual field, the geometry of the visual field intensity differs from subject to subject. For example, the "blind spot" caused by the optic nerve has a different location for each subject. In addition, the number of points observed for a given realization of the visual field ranges from 450 to 650 points between subjects. The number of points observed also depends on the choice of the threshold; the same minimum correlation threshold between the BOLD signal and the visual image is chosen for all the subjects.

Because of the variability between subjects (Figure 7), we model the intensity for a given subject,

$\lambda_i(r, \theta)$ for subject i

where r is the radius and

θ is the angle from the horizontal

are the same across scans made during the same scan session for an individual subject. In order to assess pre versus post, we also assume that without an intervention the underlying non-homogeneous Poisson process intensity does not change across sessions which may be days or weeks apart. The variability between subjects with no mask displayed in Figure 6 also shows the tendency for the pattern of points to be oval rather than completely circular. Again because of the winner take all rule and the size of the voxel measured by fMRI which often contains vasculature draining into more than one region of the brain, the "blind spot" does not provide an obvious hole in most of the subjects point patterns.
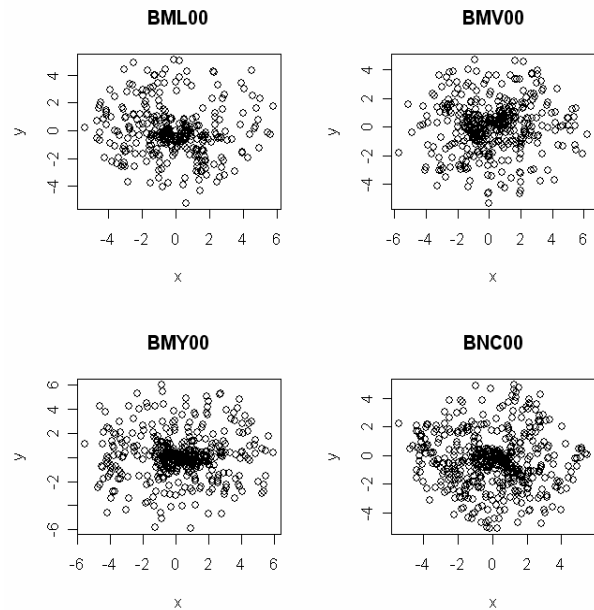
Figure 9. Variability of the pattern of points among 4 subjects.

3. Analytic Methods

3.1 Using Global Measures to Distinguish Patterns

Typical spatial statistical methods for point processes (Diggle, 2001, Waller, 2003 and Schabenberger, 2004) are designed to (1) determine how observed spatial distributions compared with a null hypothesis of Complete Spatial Randomness (CSR) and (2) to look for clusters of points as in disease mapping. Typically they assume a homogeneous Poisson spatial process with $\lambda(s)$ = constant. Since our process in non-homogeneous, we started with methods that were not dependent on the exact form of the spatial intensity. The software package R with the libraries spatstat and splancs was used for most of the analyses in this paper.

3.1.1 Nearest Neighbor Distances

The first approach was to use the distances to the nearest neighbor. The c.d.f of the <u>nearest neighbor distances</u> for each point, F(d), was computed for each visual field map. A Kolmologorov-Smirnov two-sample test of the differences between the nearest neighbor distances from the complete map compared to the distributions of the nearest neighbor differences for the 45 degree mask, the 90 degree mask and the 50% thinning was performed.

As can be seen from Figure 8, there is little difference in the nearest neighbor distances when a wedge is cut out of the mask. Although the nearest neighbor map was somewhat sensitive to thinning, it was quite insensitive to sections cut out. This method also doesn't easily lead to identification of the location of the wedge.
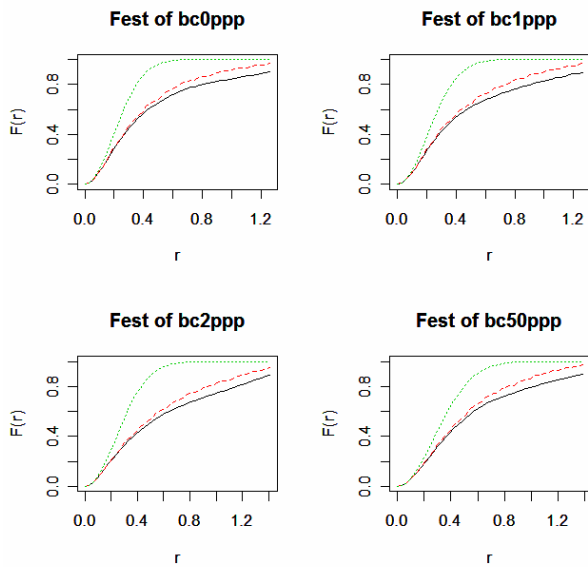
Figure 8. The distribution of the nearest neighbor distances for (0) no mask, (1) a 45 degree mask, (2) a 90 degree mask and (50) a 50% random thinning of the unmasked data.

3.1.2 Empty Space Distances

The second global method we explored was was the c.d.f of the distance from a random set of locations to the nearest point. This is called the "empty space distribution", K(d). If there are holes or masks, random locations in the hole or masked area will produce an increased distance to the nearest point. This should be more sensitive to missing areas, since random locations in the masked region should have much larger nearest neighbor distances. A Kolmologorov-Smirnov two-sample test of the differences between the nearest neighbor distances

from the complete map compared to the distributions of the nearest neighbor differences for the 45 degree mask, the 90 degree mask and the 50% thinning.
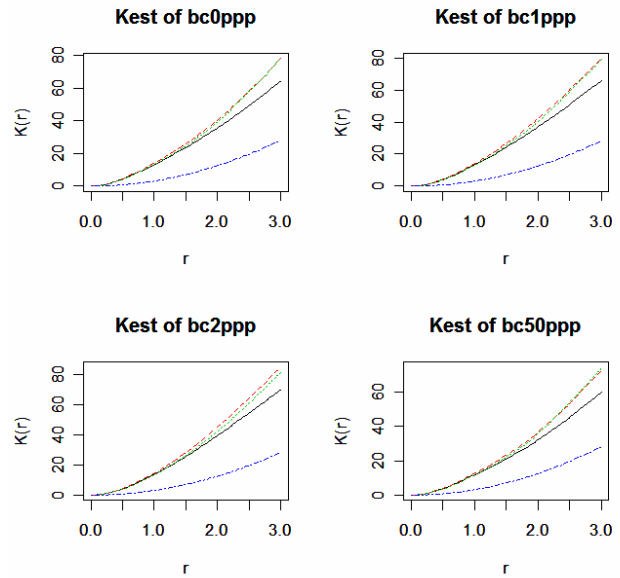
Figure 9. The distribution of the nearest neighbor distances for a random point for (0) no mask, (1) a 45 degree mask, (2) a 90 degree mask and (50) a 50% random thinning of the unmasked data.

As can be seen from Figure 9, there is little difference in the empty space distances when a wedge is cut out of the mask. Although the nearest neighbor map was somewhat sensitive to thinning, it was quite insensitive to sections cut out. This method is slightly better than the nearest neighbor method, but not much. This method also doesn't easily lead to identification of the location of the wedge.

3.2 Local Spatial Pattern Methods

The two most common methods for assessing changes (spatial-temporal) or differences (between patterns) are in terms of (1) ratios of the intensity of the two patterns – assessed with Monte Carlo sampling and (2) comparing an "expected" distribution of points based on a baseline or in our case a complete pattern of points with an "observed" number. Usually a chi-square test statistic is used to quantify this comparison.

3.2.1 Using Empirical Modeling of the First Order Intensity of the Process to Identify the Differences in Visual Field Diagrams

$\lambda(s)$ is the first order or mean of the spatial process. A homogeneous Poisson Process has

$$\lambda(s) = \lambda$$

Since the process for the visual field is non-homogeneous, choosing an underlying model for the intensity, $\lambda(s)$, is not easy. NOTE that the intensity is not monotone away from the center because of visual features like the blind spot (the optic nerve in the retina). Thus smoothing the pre-surgical observed data gives an empirical (person-specific) model to test against. To eliminate some of these problems of the different structures between subjects, the estimated ratio of the intensities was used.
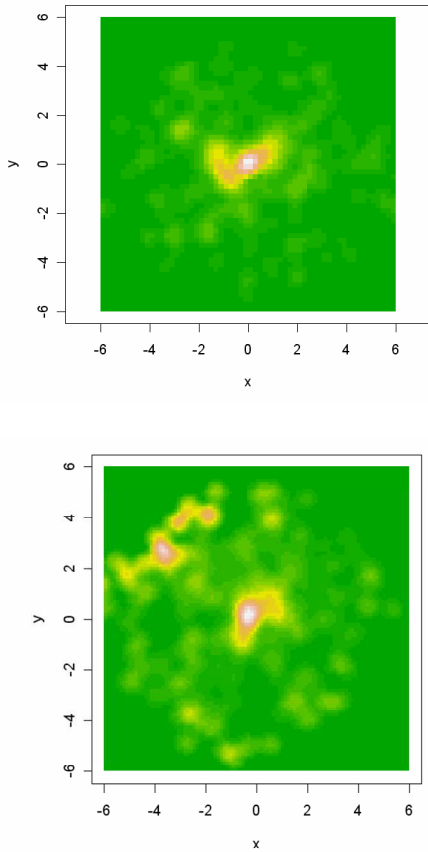
Figure 10. The effect of different smoothing parameters on the estimated spatial intensity. The bottom figure has a smaller window.

The difficulty with smoothing is that there are many parameters to choose: Window size, kernel type, and grid on which the result is plotted and displayed all can give different results for the smoothed empirical density as well as the ratio of the empirical densities.

However, Figures 11 and 12 show the best results for the intensity ratio with the full set of points and the masked set of points superimposed. Recall that each scan is a different realization of the underlying spatial stochastic process.

The results are VERY sensitive to bandwidth as well as moderately sensitive to alignment across scans and tend to overshoot near the center. The kernel type is not very important.
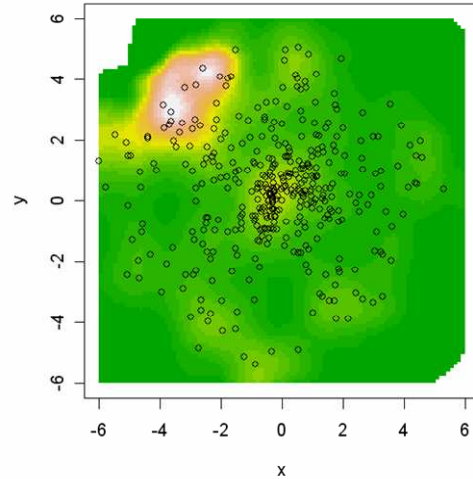
Figure 11. Empirical ratio of the intensities with the complete set of points superimposed.
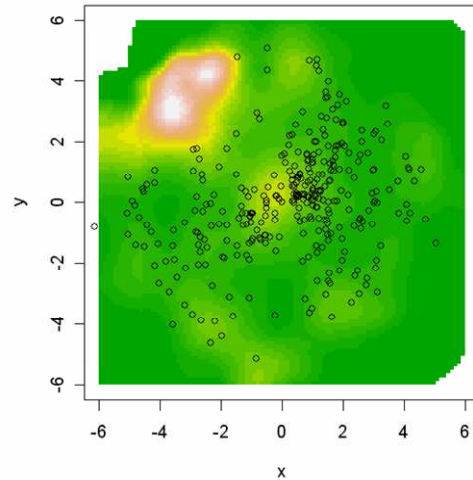
Figure 12. Empirical ratio of the intensities with the 90 degree mask set of points superimposed. The yellow-white region identifies the area where the ratio is not uniformly near a constant (green).

The main problem is the amount of tuning necessary to produce an intensity ratio that so clearly identifies the masked area. An additional problem is that kernal smoothing a spatial figure with abrupt changes in the intensity, as in the "blind spot" has tendency to produce overshoot of the estimated intensity.

Perhaps a 2D Haar wavelet smoother would be more successful at modeling the local variation without overshoot than a kernal smoother..

This method successfully identified holes; for thinning it should produce a more or less constant ratio of intensities. However the ratio will be offset from 1, the expected ratio in regions with no holes.

We used the R library splancs for smoothing kernels and estimating ratios of smoothed kernels

3.2.2 Using the Full Scan to Determine a Predicted Number of Pointes to Compare with the Observed Number of Points.

This method partitions the visual field map into reproducible areas. Although there are many potential ways to partition the visual field map, we invoke two constraints that lead to fewer choices. The first is to be sure that for all subjects we have an expected number greater than or equal to five so that there will be no problem with the estimation of the expected value. The second is that the each partition should have about the same number of points. This leads to a series of wedges or a series of unequally sized annuli that take into account the increased density towards the center of the visual field map (Figure 13). We then used a Pearson's Chi-square test statistic to test whether there are any differences in the patterns among the sectors.
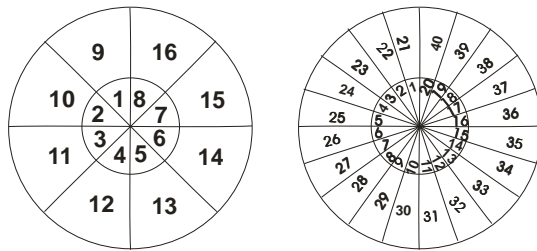
Figure 13. Partitioning of the visual field into wedges that will have similar numbers of points.

The increased sized for the outer wedges corresponds to the decreased density of the points, as well as the corresponding decrease in visual acuity. The number of sectors allows us to tune the sensitivity of the method by adjusting the number of points in a wedge. A method that is too sensitive will differentiate between identical scans from different sessions. A method that is not sensitive enough will only differentiate very large holes.

The additional advantage of more and smaller wedges is that the "blind spot" can easily be omitted if it is

causing spurious significance without affecting the ability to detect the location of holes and thinning.

The z-score for each sector can be used to locate the deviant sectors. Bigger annuli are needed as the points thin out.

Partitioning the visual field into wedges or annuli was (1) very sensitive to big cutouts and less sensitive to small cutouts, (2) very sensitive to thinning and (3) very sensitive to differences between subjects. We noticed that it needs careful alignment of the voxels of the visual cortex to be useful in tracking results of sessions that are collected over long periods of time. We are still working on the sensitivity problem. The choice of nested annuli may be optimal if the region of vision loss tends to occur towards the outside of the visual field.

Acknowledgements

References

DeYoe EA., Carman G., et al. (1996). "Mapping striate and extrastriate visual areas in human cerebral cortex." Proceedings of the National Academy of Sciences - USA 93(6): 2382-2386.

DeYoe EA., Williams K, et al. (1997). "FMRI-based "functional field maps" of brain-related vision defects." Society for Neuroscience Abstracts 23: 1403.

Maciejewski M., Ropella KM, et al. (2005). Combining fMRI with Video Automated Perimetry in Patients with Brain-based Visual Impairments. IEEE EMBS Conference on Neural Engineering, Arlington, VA

Hoffmann RG "Techniques for fMRI Visual Field Diagram Analysis" Proceeding of the American Statistical Association, 2004.

Hoffmann RG, Deyoe EA, Brefcynski J, Thakkur M, Rowe DB. "Spatial-Temporal Models for Visual Field Pathology". Proceeding of the American Statistical Association, 2005.

Diggle, PJ. Statistical Analysis of Spatial Point Patterns. Oxford University Press. 2001. London.

Schabenberger O and Gottway C. Statistical Methods for Spatial Data Analysis. 2004. CRC Press. New York.

Bailey TC and Gatrell AC. Interactive Spatial Data Analysis. Prentice-Hall. 1996. New York.

Waller L and Gottway C. Applied Spatial Analysis of Public Health Data. John Wiley and Sons. 2003. New York.